Eur. Phys. J. C (2005)
Digital Object Identifier (DOI) 10.1140/epjc/s2005-02194-0

THE EUROPEAN PHYSICAL JOURNAL C

In-medium spectral functions from lattice QCD

Tetsuo Hatsuda[a]

Department of Physics, The University of Tokyo, 7-3-1, Hongo, Bunkyo-ku, Tokyo 113-0033, Japan

Received: 14 February 2005 /
Published online: 14 April 2005 –

Abstract. Hadronic modes in the quark–gluon plasma and their spectral properties are discussed on the basis of the lattice QCD data analyzed by the maximum entropy method.

PACS. 12.38.Mh, 12.38.Gc

1 Introduction

Properties of the hot hadronic and quark–gluon plasma may be probed by the in-medium modification of hadronic excitations as discussed in [1–5] (see also the reviews in [6]). In particular, it was argued in [2, 3] that soft hadronic modes survive even in the quark–gluon plasma (QGP) at temperature (T) higher than the critical temperature (T_c). The idea can be best summarized as follows: "... there arise soft modes having a large strength and a narrow width above the critical temperature, which are analogous to the fluctuation of the order parameter in a superconductor above the critical point" (from the abstract of [2]), and "... the plasma exhibits confining features similar to that of the low-temperature hadronic phase. The confining features are manifest in the long-range, i.e., long-wavelength, low-frequency, modes of the plasma" (from the abstract of [3]).

Shown in Fig. 1 is an example of the spectral function (SPF) of the chiral soft modes (σ and π) at $T > T_c$ obtained in the Nambu–Jona–Lasinio model [2]. One finds that a low mass and narrow width peak develops towards T_c, which is later called the "para-pion" (a soft excitation in the para-phase of chiral symmetry) [7].

Although many studies on the basis of model Lagrangians have been carried out for the hadronic modes at finite T, the first principle lattice QCD analysis became possible only recently: A key observation is the use of the maximum entropy method (MEM) [9,10]. In the following, we summarize our results on the bound states of heavy and medium-heavy quarks such as J/Ψ, η_c and ϕ above the deconfinement temperature in quenched QCD.

2 QCD spectral functions at finite T

Let us consider the spectral function $A(\omega, \boldsymbol{p})$ defined as the imaginary part of the retarded correlation of a hadronic interpolating field $J(x)$. For the vector mesons, we have

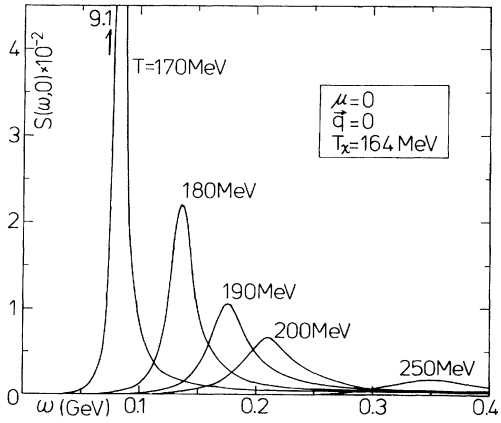

Fig. 1. The dynamic structure factor $S(\omega)$ as a function of frequency ω in the (σ, π) channel above the critical temperature of chiral phase transition in the two-flavor Nambu–Jona–Lasinio model [2]. Quark masses are taken to be zero. A soft and narrow-width collective mode develops as T approaches to the critical temperature $T_c \simeq 164\,\mathrm{MeV}$

$J = \bar{c}\gamma_\mu c$ for J/ψ, $J = \bar{s}\gamma_\mu s$ for the ϕ-meson, $J = \frac{1}{2}(\bar{u}\gamma_\mu u - \bar{d}\gamma_\mu d)$ for the ρ^0-meson, and $J = \frac{1}{2}(\bar{u}\gamma_\mu u + \bar{d}\gamma_\mu d)$ for the ω-meson. Both the real-time (retarded) and imaginary-time (Matsubara) correlations can be reconstructed from $A(\omega, \boldsymbol{p})$ through the dispersion relation.

Next we introduce the Matsubara correlation $D(\tau, \boldsymbol{p})$ in a mixed representation:

$$D(\tau, \boldsymbol{p}) = \int \mathrm{d}^3x\ \mathcal{D}(\tau, \boldsymbol{x}) \mathrm{e}^{-\mathrm{i}\boldsymbol{p}\cdot\boldsymbol{x}}, \tag{1}$$

where $\mathcal{D}(\tau, \boldsymbol{x})$ is an imaginary-time correlation function. Carrying out the Fourier transform, one arrives at

$$D(\tau, \boldsymbol{p}) = \int_{-\infty}^{+\infty} \frac{\mathrm{e}^{-\tau\omega}}{1 \mp \mathrm{e}^{-\beta\omega}}\ A(\omega, \boldsymbol{p})\ \mathrm{d}\omega \quad (0 \le \tau < \beta), \tag{2}$$

Equation (2) is always convergent for $\tau \neq 0$ as long as $A(\omega \to \infty, \boldsymbol{p})$ does not grow exponentially.

[a] e-mail: hatsuda@phys.s.u-tokyo.ac.jp

3 Maximum entropy method

Lattice Monte Carlo simulations provide $D(\tau, \boldsymbol{p})$ on a discrete and finite set of τ and $\boldsymbol{p}$. From such numerical data, we need to extract the spectral function A being a continuous function of ω. This is a typical ill-posed problem, where the number of data points is much smaller than the number of degrees of freedom to be reconstructed. The standard χ^2-fitting is obviously inapplicable here, since many degenerate solutions appear in minimizing χ^2.

One way to avoid this problem is to introduce an ansatz for the spectral function with a few parameters [11]. However, the spectral structure at finite T is not known in general. MEM is an approach to circumvent this difficulty on the basis of the Bayesian probability theory [8]. In MEM, we do not need to introduce a priori assumptions or parameterizations of the spectral functions. Nevertheless, for given lattice data, a unique solution is obtained if it exists. Furthermore, one can evaluate the statistical significance of the results.

In MEM, the most probable A given lattice data D is obtained by maximizing the conditional probability

$$P[A|D] \propto \mathrm{e}^{\alpha S - L}, \tag{3}$$

where L is the standard likelihood function and S is the Shannon–Jaynes entropy [12]:

$$S = \int_0^\infty \left[A(\omega) - m(\omega) - A(\omega) \log \left(\frac{A(\omega)}{m(\omega)} \right) \right] \mathrm{d}\omega. \tag{4}$$

Here α is a parameter dictating the relative weight of S and L. The statistical significance (error) of the resultant A is estimated by the second variation, $(\delta/\delta A)^2 P[A|D]$. The default model m in (4) may be chosen so that the MEM errors become minimum. The final result is given by the weighted average over α as

$$A(\omega, \boldsymbol{p}) = \int A_\alpha(\omega, \boldsymbol{p})\ P[\alpha|Dm]\ \mathrm{d}\alpha, \tag{5}$$

where $A_\alpha(\omega, \boldsymbol{p})$ is obtained by minimizing $P[A|D]$ for a fixed α. The conditional probability $P[\alpha|Dm]$ can be calculated by using the Bayes theorem and the lattice data. Thus α is eventually integrated out and does not appear in the final result.

A first successful application of MEM to the lattice QCD data at $T = 0$ has been done for the ground and excited meson spectra [9]. Also, basic concepts and techniques of MEM applied to lattice QCD have been summarized in [10].

Shown in Fig. 2 is a first spectral image of the vector meson at rest ($\boldsymbol{p} = 0$) extracted from the quenched QCD data generated on a $20^3 \times 24$ lattice with $\beta = 6/g^2 = 6.0$. Here a dimensionless spectral function $\rho(\omega) = A(\omega, \boldsymbol{0})/3\omega^2$ is introduced. The first (second) peak corresponds to the ground (excited) vector meson. On the other hand, the highest peak corresponds to a bound state of Wilson doublers as argued in [13]. MEM has been also applied to the ground and excited baryons in [14]. Shown in Fig. 3 is the spectral function in the nucleon channel extracted from the quenched QCD data generated on a $32^3 \times 32$ lattice with $\beta = 6.0$. The first (second) peak corresponds to the nucleon and the Roper resonance, while the higher two peaks correspond to the bound states of Wilson doublers [15].

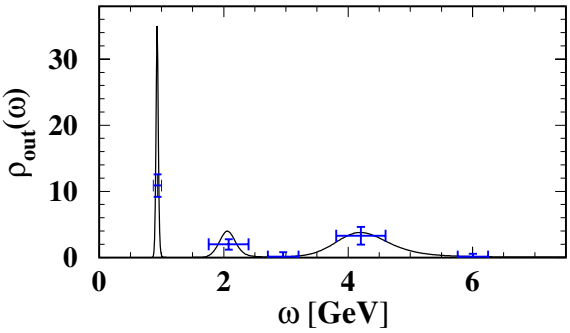

Fig. 2. The dimensionless spectral function $\rho(\omega) = A(\omega, \boldsymbol{0})/(3\omega^2)$ of the vector meson extracted from a $20^3 \times 24$ lattice with $\beta = 6.0$ ($a \simeq 0.085\,\mathrm{fm}$). The hopping parameter is taken to be $\kappa = 0.1557$. The figure is taken from [9]

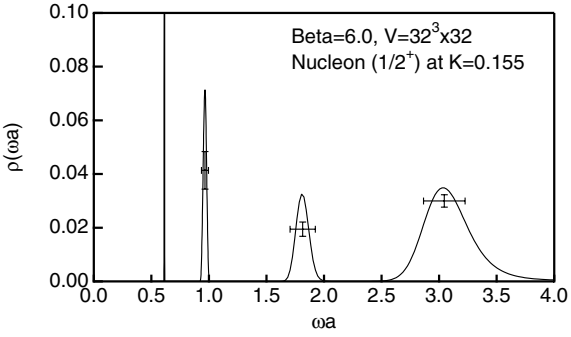

Fig. 3. The dimensionless spectral function $\rho(\omega) = A(\omega, \boldsymbol{0})/\omega^5$ in the nucleon channel extracted from a 32^4 lattice with $\beta = 6.0$. The horizontal axis denotes a dimensionless frequency ωa. The figure is taken from [14]

4 Anisotropic lattice

When we apply MEM to the system at finite T, there arises a difficulty originating from the fact that the temporal lattice size L_τ is restricted as $L_\tau = 1/T = N_\tau a_\tau$. Here a_τ (N_τ) is the temporal lattice spacing (the number of temporal lattice sites). Because of this problem, it becomes more difficult to keep enough N_{data} to obtain reliable SPFs as T increases. In other words, simulations up to a few times T_{c} with N_{data} as large as e.g. 30 require a fine lattice in the temporal direction. This naturally leads us to the use of the anisotropic lattice where temporal lattice spacing a_τ is smaller than the spatial lattice spacing a_σ.

In [16], we have carried out a quenched QCD simulations with $\beta = 7.0$ on $32^3 \times N_\tau$ anisotropic lattice with the renormalized anisotropy $\xi = a_\sigma/a_\tau = 4.0$. We take the naive plaquette gauge action and the standard Wilson quark action. The fermion anisotropy $\gamma_F \equiv \kappa_\tau/\kappa_\sigma$ with κ_σ (κ_τ) being the spatial (temporal) hopping parameter is determined by comparing the temporal and spatial effective masses of the pseudo-scalar and vector mesons on

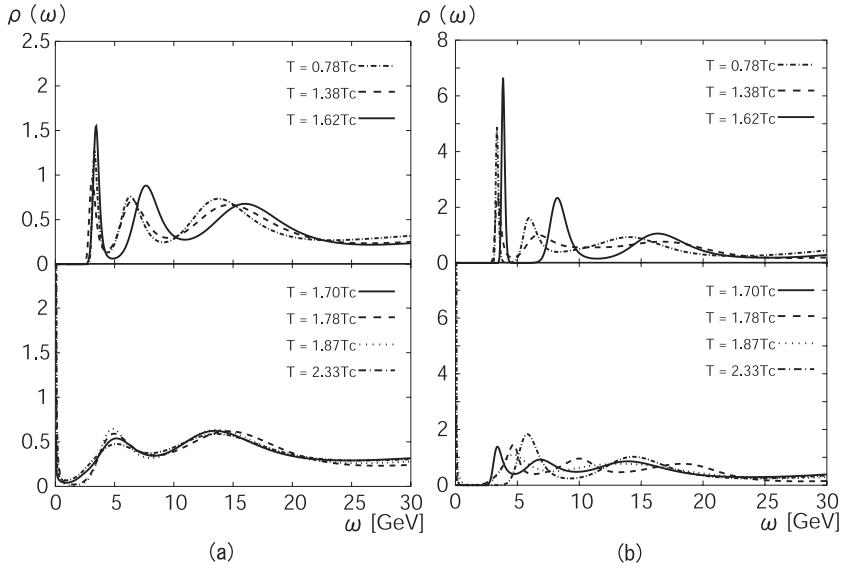

Fig. 4. The dimensionless spectral function $\rho(\omega)$ measured on an anisotropic lattice in (a) the J/Ψ channel and in (b) the η_c channel. See Sect. 4 for lattice parameters. The data are taken from [16]

Table 1. Number of spatial lattice points N_τ and corresponding temperature divided by T_c. The number of gauge configurations $N_{\rm gauge}$ for each T is also given

N_τ	96	54	46	44	42	40	32
T/T_c	0.78	1.38	1.62	1.70	1.78	1.87	2.33
$N_{\rm gauge}$	194	150	182	180	180	181	141

a lattice $V = 32^2 \times 48 \times 128$. The lattice spacing is determined from the ρ-meson mass in the chiral limit, which gives $a_\tau = a_\sigma/4 = 9.75 \times 10^{-3}$ fm. The physical lattice size in the spatial direction reads $L_\sigma = 1.25$ fm. The masses determined on the $T = 0$ lattice are

$$m^{\rm lat}_{J/\psi} \simeq 3.10\,{\rm GeV}, \quad m^{\rm lat}_{\eta_c} \simeq 3.03\,{\rm GeV}, \tag{6}$$

which should be compared with the experimental values, 3.10 GeV and 2.98 GeV, respectively.

At finite T, the Polyakov-loop susceptibility has a sharp peak around $N_\tau = 80$ (72), which corresponds to $T_c = 253$ (281) MeV, consistent with the known T_c in pure gauge theory, 271 ± 2 MeV. N_τ, the corresponding T/T_c, and the number of gauge configurations $N_{\rm gauge}$ are summarized in Table 1. Gauge configurations are generated by the pseudo heat-bath and over-relaxation algorithms with a ratio 1 : 4. Initially, the gauge field is thermalized with 10 000 sweeps and, then each configuration is separated by 1000 sweeps.

5 Charmonia at $T \neq 0$

Let us discuss some of the interesting features of Fig. 4. The dimensionless SPFs are defined as $\rho(\omega) = A(\omega, \mathbf{0})/\omega^2$ for η_c and $\rho(\omega) = A(\omega, \mathbf{0})/(3\omega^2)$ for J/ψ.
(1) If the deconfined plasma were composed of almost free quarks and gluons, SPFs would show a smooth structure with no pronounced peaks above the $q\bar{q}$ threshold. To the contrary, we find a sharp peak near the zero-temperature mass even up to $T \simeq 1.62T_c$ as shown in Fig. 4 [16]. Also we found that the peak disappears suddenly above $T \simeq 1.7T_c$. The existence of the charmonium bound state above T_c was also observed by Umeda et al. [17] and by Datta et al. [18].
(2) The width of the first peak in Fig. 4a partly reflects the unphysical broadening due to the statistics of the lattice data and partly reflects possible physical broadening at finite T. At the moment, the former width dominates and we are not able to draw definite conclusions on the thermal mass shift and broadening.
(3) The second and third peaks in Fig. 4 may be related to the fermion doublers originally discussed in [13]. This must be checked, however, by studying the scaling of the peak position as $1/a_\sigma$.

6 Reliability tests in MEM

Any spectral functions on the lattice obtained from MEM need to pass several validity tests. This is important because the lack of accurate lattice data can cause fake peaks and/or fake smearing as demonstrated by the mock data in [10].
(1) Among others, the first test is the error analysis of the peaks from the second variation, $\delta^2 P[A|D]/\delta A(\omega)\delta A(\omega')$. It has been checked that the sharp peak at $T = 1.62T_c$ in Fig. 4 is statistically significant. The absence of a peak at $T = 1.70T_c$ is also statistically significant. The same features are also observed for η_c.
(2) The second test is for the dependence of the SPFs on the variation of the number of data point $N_{\rm data}$ employed for the MEM analysis. In particular, one should use the same $N_{\rm data}$ to extract the spectral function for different T. Otherwise, one cannot know whether the disappearance of a peak is due to the real thermal effect or from the artifact

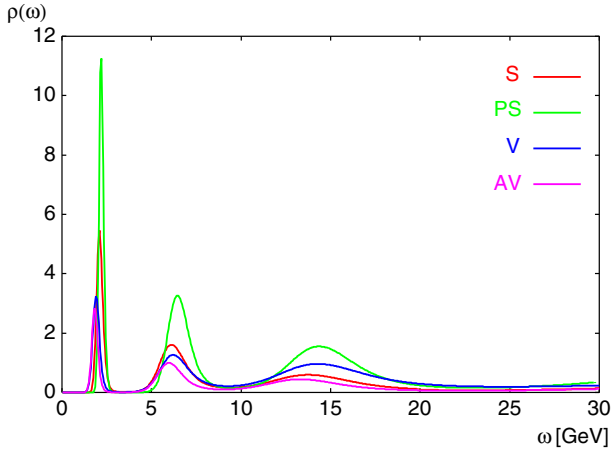

Fig. 5. SPFs for the $s\bar{s}$-mesons at $T/T_c = 1.38$. The figure is taken from [19]

of insufficient number of $N_{\rm data}$. This has been checked carefully to ensure that the sudden disappearance of the J/Ψ and η_c peaks is real.
(3) The third test which is not done yet with our data is a study of the finite volume effect. The spatial volume of our lattice is about 1.25 fm which is lager than the 1 fm diameter of J/Ψ at $T = 0$ but may not be large enough for the loosely bound charmonium above T_c. The effect of the finite spatial volume on the SPFs in Fig. 4 is one of the most important problems to be studied.

7 Strange mesons at $T \neq 0$

Shown in Fig. 5 is the SPFs of the $s\bar{s}$-mesons in the scalar (S), pseudo-scalar (PS), vector (V) and axial-vector (AV) channels [19]. The temperature is taken to be $T/T_c = 1.38$ and the quark mass is chosen to reproduce the experimental ϕ-meson mass at $T = 0$ approximately.

In this case, one finds that SPFs in all channels have degenerate peaks around 2.5 GeV. Also, such sharp peaks disappear at high enough temperature, e.g. at $T/T_c = 1.87$.

8 Effect of dynamical quarks

The results of the SPFs shown in Figs. 4 and 5 are obtained in the quenched approximation in which dynamical quarks (both quantum and thermal ones) are neglected. Namely, they are the results in the gluon plasma and not in the quark–gluon plasma. Now what would happen if the dynamical quarks are included?

One can immediately imagine several dynamical effects. A first one is an effect which tends to destroy the hadronic resonance above T_c due to its collisions with dynamical quarks. The second one is an effect which tends to reduce such collisional effect due to the reduction of the critical temperature ($T_c^{\rm quenched} \sim 270\,{\rm MeV} \to T_c^{\rm full} \sim 170\,{\rm MeV}$). The ratio of the dissociation rate between quenched QCD and full QCD around T_c may be roughly estimated by the number of active degrees of freedom in the plasma:

$$\frac{n_{q+g}(T_c^{\rm full})}{n_g(T_c^{\rm quench})} = \frac{16+21}{16}\left(\frac{T_c^{\rm full}}{T_c^{\rm quench}}\right)^3 \simeq 0.62, \qquad (7)$$

where we have taken $N_f = 2$. Namely, the net thermal dissociation rate of the resonance may be weaker in full QCD than in quenched QCD.

Whether this expectation is valid or not should be studied by the future full QCD simulations at finite T.

9 Summary and concluding remarks

We have discussed our recent studies on the hadronic modes above the critical temperature of the QCD phase transition. In the quenched QCD on the lattice, J/Ψ and η_c are shown to survive even at $T/T_c = 1.62$ but they disappear rather abruptly above $T/T_c = 1.7$.

If there exist hadronic modes above T_c, what would be the physics behind them? To unravel the true nature of such modes, it is important to extract detailed information such as the spatial correlation function between the quark and the anti-quark on the lattice [20] and the color-singlet quark–anti-quark potential on the lattice [21]. Also the phenomenological studies such as discussed in [22, 23] are useful to interpret the lattice results.

References

1. R.D. Pisarski, Phys. Lett. B **110**, 155 (1982)
2. T. Hatsuda, T. Kunihiro, Phys. Rev. Lett. **55**, 158 (1985)
3. C. DeTar, Phys. Rev. D **32**, 276 (1985)
4. T. Hashimoto, K. Hirose, T. Kanki, O. Miyamura, Phys. Rev. Lett. **57**, 2123 (1986)
5. T. Matsui, H. Satz, Phys. Lett. B **178**, 416 (1986)
6. T. Hatsuda, T. Kunihiro, Phys. Rept. **247**, 221 (1994); G.E. Brown, M. Rho, Phys. Rept. **269**, 333 (1996)
7. T. Hatsuda, talk at 9th Nishinomiya-Yukawa Memorial Symposium: Relativistic Cosmology (Nishinomiya, Japan, 1994); hep-ph/9502345
8. B.R. Frieden, J. Opt. Soc. Am. **62**, 511 (1972); N. Wu, The maximum entropy method (Springer-Verlag, Berlin 1997)
9. Y. Nakahara, M. Asakawa, T. Hatsuda, Phys. Rev. D **60**, 091503 (1999)
10. M. Asakawa, T. Hatsuda, Y. Nakahara, Prog. Part. Nucl. Phys. **46**, 459 (2001)
11. T. Hashimoto, A. Nakamura, I.O. Stamatescu, Nucl. Phys. B **400**, 267 (1993); B **406**, 325 (1993)
12. C.E. Shannon, W. Weaver, The mathematical theory of communication (Univ. of Illinois Press, Urbana 1949); E.T. Jaynes, Phys. Rev. **106**, 620 (1957); **108**, 171 (1957)
13. T. Yamazaki et al. (CP-PACS Collaboration), Phys. Rev. D **65**, 014501 (2002)
14. K. Sasaki, S. Sasaki, T. Hatsuda, M. Asakawa, Nucl. Phys. Proc. Suppl. **129**, 212 (2004)
15. K. Sasaki, S. Sasaki, T. Hatsuda, in preparation
16. M. Asakawa, T. Hatsuda, Phys. Rev. Lett. **92**, 012001 (2004); J. Phys. G **30**, S1337 (2004)

17. T. Umeda, K. Nomura, H. Matsufuru, Eur. Phys. J. C 10.1140/epjcd/s2004-01-002-1 (2004); hep-lat/0501002
18. S. Datta, F. Karsch, P. Petreczky, I. Wetzorke, Phys. Rev. D **69**, 094507 (2004)
19. M. Asakawa, T. Hatsuda, Y. Nakahara, Nucl. Phys. Proc. Suppl. **119**, 481 (2003); Prog. Theor. Phys. Suppl. **149**, 42 (2003)
20. Ph. de Forcrand et al. (QCD-TARO Collaboration), Phys. Rev. D **63**, 054501 (2001)
21. A. Nakamura, T. Saito, Prog. Theor. Phys. **111**, 733 (2004), and references therein
22. S. Digal, P. Petreczky, H. Satz, Phys. Lett. B **514**, 57 (2001)
23. G.E. Brown, C.-H. Lee, M. Rho, E. Shuryak, Nucl. Phys. A **740**, 171 (2004); E.V. Shuryak, I. Zahed, Phys. Rev. D **70**, 054507 (2004)